Electrical Imaging of the Intracratonic Parnaíba Basin, North-Northeast Brazil

B. R. Arora[1,*], A. Rigoti[2], Í. Vitorello[1], A. L. Padilha[1], N. B. Trivedi[1], and F. H. Chamalaun[3]

[1]*Instituto Nacional de Pesquisas Espaciais - INPE, C.P. 515, 12201-970 São José dos Campos, Brazil*
[2]*Departamento de Geologia, Universidade Federal do Paraná, C.P. 19011, 81531-990 Curitiba, Brazil*
[3]*School of Earth Sciences, Flinders University of South Australia, G.P.O. Box 2100, Adelaide, S.A., 5001, Australia*

(Received November 7, 1996; Revised July 25, 1997; Accepted July 30, 1997)

Nighttime transient geomagnetic variations recorded by an array of 29 magnetometers in the equatorial region of north-northeast Brazil have been subjected to robust regression analysis in order to derive transfer functions as a diagnostic indication of lateral conductivity variations. A thin sheet conductance model was developed to explain and interpret the variety of conductive anomalies evidenced by the induction arrow maps. The two main structures revealed by the present study are: a large NE-SW trending conductive anomaly with an embedded resistive zone in the central part of the Parnaíba Basin (Parnaíba Basin Conductive Anomaly—PBCA) and a relatively weaker anomaly branching off from the northwestern corner of the PBCA and extending towards the Marajó basin (LINK anomaly). The major PBCA anomaly is provisionally interpreted as a graben in the Precambrian basement filled with carbonaceous carbonates. The embedded resistive body, also characterized by a high density, is shown to be consistent with the presence of a diabase intrusive related to a magmatic event. The LINK anomaly is tentatively considered to be the relics of a sedimentary channel connecting the Parnaíba and Marajó basins.

1. Introduction

The Phanerozoic sedimentary sequence, covering almost one third of the entire Brazilian territory, is largely composed of three intracratonic basins: Amazon, Parnaíba and Paraná (Almeida *et al.*, 1981)—see inset in Fig. 1 for locations. The present paper is concerned with a large-scale magnetometer array study, aimed at the electrical imaging of the Parnaíba basin. Located in the north-northeast Brazil with an area of roughly 600,000 km^2, the basin is also known as the Maranhão basin. As yet, most of the information on the sedimentary sequence has come from the geological mapping of the outcrops and from a few exploratory boreholes drilled by PETROBRÁS (Petróleo Brasileiro S.A.) to evaluate the hydrocarbon prospects. The geology and sedimentation history of the Parnaíba basin have extensively been discussed by Mesner and Wooldridge (1964) and Bigarella (1973) and have recently been updated by Góes *et al.* (1990) in the light of updated information. The basin is mainly filled with Paleozoic sediments, although a large area, especially in the northwestern part, is covered by a thin layer of Mesozoic sediments. Sedimentation extending from the Ordovician to the Tertiary has occurred in three megacycles represented respectively by the Serra Grande (Ordovician-Silurian), Canindé (Devonian) and Balsas (Triassic-Cretaceous). Each group is separated by widespread regional discordances, signifying slow epeirogenic movements in the evolution of the basin. During the Jurassic and early Cretaceous, the basin experienced a major magmatic event and sedimentary columns were extensively intruded by diabase dikes, and large volumes of basalts were extruded. Even though the stratigraphy and sedimentation history are reasonably understood, there is much about the

*Permanently at: Indian Institute of Geomagnetism, Colaba, Mumbai 400005, India

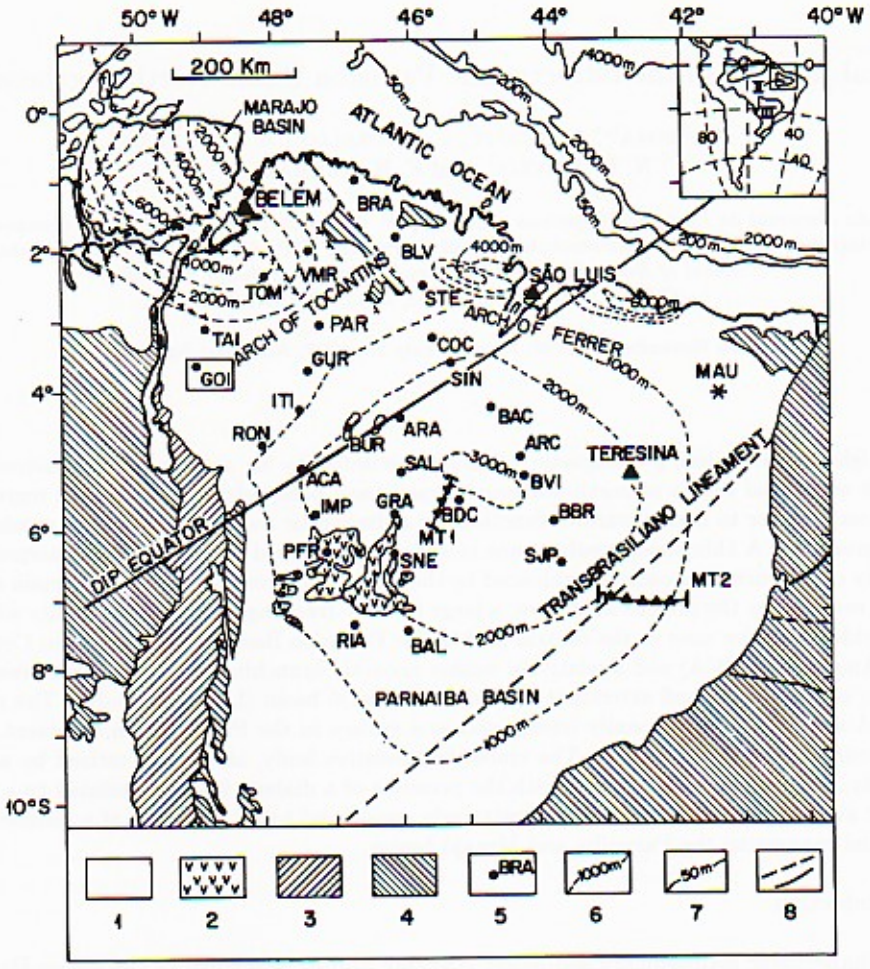

Fig. 1. Map showing the layout of magnetometer sites in relation to general geology of the study area (DNPM, 1971), where marked legends represent: (1) Phanerozoic sediments, (2) Mesozoic volcanics, (3) Araguaia fold belt, (4) undifferentiated Precambrian, (5) magnetometer sites, (6) sediment thickness, (7) ocean depth, and (8) trace of faults. Locations of magnetotelluric profiles (MT1 and MT2) referred to in the text are also shown. Inset shows the location of the study area and three intracratonic basins namely: I - Amazon; II - Parnaíba and III - Paraná.

geology of the basin that is in dispute or not properly known. Although the evolution of the basin is related to marine transgressions and regressions, the near oval shape of the basin with no well defined axis of deposition gives no clue on the direction of sea intrusion. It is also not clear whether the Parnaíba basin was interconnected to the other intracratonic basins during the different phases of the basin evolution. The basement as well as the deeper crustal structures are poorly known and the information on the control of Precambrian tectonic elements of the region on the evolution of the basin is almost totally missing. The geophysical investigations, including gravity, aeromagnetic, magnetotelluric and seismic, launched to image the deeper structures as an aid to the tectonic evolution history, are on different stages of data collection but their qualitative evaluation suggests a complex structural setting at depth (Nunes, 1993). The present exercise, to delineate and map the internal and basement structure of the basin in terms of electric

conductivity, is expected to complement these ongoing geophysical investigations. In this paper, summarizing the salient induction features deduced from the analysis of the transient geomagnetic variations recorded by the array of magnetometers, lateral depth-integrated conductance distribution is derived. Tectonic implications of the mapped conductivity structures in the evolution of the Parnaíba basin are discussed in the context of the results.

2. Array Configuration and Geological Setting

Figure 1 shows the layout of the magnetometer sites in relation to the major geological and tectonic features of N-NE Brazil. A large part of the study area falls under the influence of the intense band of Equatorial Electrojet (EEJ) currents, centered at the dip-equator. With most of the stations located in the oval shaped Parnaíba basin, roughly aligned along three profiles perpendicular to the dip equator, the array presented reasonable distribution of stations for both EEJ and induction studies using the principles of geomagnetic deep soundings (GDS). The chain of stations, BLV-STE-COC-SIN-BAC-ARC-BVI-BBR-SJP, located along the northeastern part of the array where the most significant induction pattern is observed, will henceforth be referred to as the eastern profile.

In the NW of the studied area, the magnetometer coverage extended up to the southeastern limits of the Marajó basin, which is separated from the Parnaíba basin by the Arch of Tocantins and on the west is separated from the Amazon basin by the Arch of Gurupa (Rezende and Ferradaes, 1971). Structurally, the Marajó basin is a large graben bounded by a system of normal faults. To the north of the Parnaíba basin, across the Arch of Ferrer, are located the small marginal São Luiz and Barreirinha basins. All these three adjoining basins, formed following the opening of the Atlantic ocean, carry thick successions of Mesozoic and Cenozoic sediments. Paleozoic sediments are also believed to be preserved in the graben under a Cretaceous cover, at least in the Marajó and São Luiz basins (Mesner and Wooldridge, 1964; Bigarella, 1973). Further to the northeast, concentration of the induced currents in the Atlantic ocean are expected to influence the geomagnetic variations recorded by the array stations. NE-SW trending Transbrasiliano Lineament, identified as a massive complex system of faults, folds and grabens (Cunha, 1986; Sousa and Oliveira, 1995), is the most dominant tectonic element flanking the array on the southeast. In the west and southwest, the magnetometer setup stands near the Araguaia fold belt, a Proterozoic suture separating the Archean Amazonic Craton from the Parnaíba basin (Almeida, 1974).

3. Data Collection and Processing

In the present study, the upgraded Flinders' set of portable fluxgate magnetometers (Chamalaun and McKnight, 1993) were deployed for data acquisition. The array recording commenced on November 22, 1990 and ended with slightly varying cut-off dates some time in the month of March, 1991. Simultaneously functioning magnetometers measured total field values of vertical (Z) and two orthogonal horizontal components at 1 minute interval. The mutually orthogonal horizontal sensors, when buried in the ground for field operation, were not aligned in any specific orientation (Chamalaun and Walker, 1982). Instead, two recorded horizontal components were combined to give resultant horizontal (H) field. Using the IGRF declination (D) value at magnetometer site, the H value was projected to provide geographic northward (X) and eastward (Y) components. The Z component was directly measured as the magnetometers were properly leveled. The data sets were edited and corrected for spurious jumps prior to further processing. Complete operational details, data quality and reduction steps are given in Rigoti (1994).

The assumption of spatially uniform source is fundamental to the identification and interpretation of anomalous magnetovariational (MV) fields towards the determination of lateral conductivity distribution. Over the present array, the presence of EEJ during daytime makes the external source field highly non-uniform. However, during the nighttime, in the absence of the EEJ, the MV fields are predominantly of magnetospheric origin and can be considered uniform at least for the dimension of the array. The MV fields recorded in the interval of 8.5 hours, centered at local midnight, were used to compute period-dependent transfer-functions, as a diagnostic indication of lateral conductivity distribution (Schmucker, 1970; Beamish, 1977). The length of the nighttime segments, each one with 512 min values, was adequate to resolve signals in the period range of a few minutes to 2–3 hours for the purpose of computing transfer functions under the assumption of a uniform source. In any case, at periods greater than 2–3 hours, the assumption of a uniform source becomes questionable due to the contamination from the harmonics of solar quiet-day variations. Within these constraints, the vertical field transfer-functions summarizing the relation between anomalous vertical and normal horizontal field components were computed for 13 period bands from 6 min to 132 min.

During the quiet periods, amplitudes of signals in these period range often drop below the system noise level. On the other hand, the assumption of uniform source fields is likely to be violated during intervals of very intense magnetic activities (Egbert and Booker, 1986). Therefore, only moderately active nighttime segments, exhibiting a wide range of frequencies and polarizations, were used for the estimation of the transfer-functions. The selection of segments was accomplished by visual inspection of data in the time domain in conjunction with the variance index for each nighttime segment. The nighttime segments whose variances were outside the empirically determined lower and upper threshold were excluded from the analysis. The selected nighttime segments were detrended and, after the removal of the mean, were joined together into a single time series to evaluate inter-station transfer function, using the robust regression technique developed by Egbert and Booker (1986). Initial examination of data in the form of Fourier Transform maps had shown that the fields at station GOI were largely free from the effects of current concentration in the anomalous zones. Therefore, the horizontal variations at station GOI were used as a measure of normal fields for the purpose of computing common reference-site (inter-station) transfer functions for all array sites. The advantage of common reference-site transfer functions as against the single-site transfer functions has been discussed by Beamish and Banks (1983).

As a first step of robust processing, a 128-point window was used to compute the fast Fourier transform (FFT). Successive windows were overlapped by 25% to increase estimation efficiency without affecting the independence of adjacent windows (Thompson, 1982). Three level decimation by a factor of four was successively used so that a fixed 128-point window enabled the estimation of transfer functions for the 13 bands. For all decimation levels, transfer functions were computed for non-overlapping bands whose widths were 25% of the central frequency. For most stations, some 51 nighttime segments were combined and it provided enough degrees of freedom for reliable statistical estimation of transfer functions for all period bands. Only at a few stations, due to loss of data for technical/accidental or occasional malfunctioning of the instruments a slightly smaller number of segments entered the computation. The number of events included for station BVI was 40, VMR, SAL, and PFR all had 31, whereas IMP had only 13 segments. Transfer functions at the reference site GOI were computed for each individual set of data of varying lengths and were found to have nearly the same values in each period bands (except at long periods when only 13 segments were used). This exercise showed that the transfer functions computed with slightly different lengths of data at various stations led to stable estimations and could be combined to delineate the regional picture of the conductivity distribution. To infer the internal conductivity distribution, vertical field transfer functions are combined in the conventional manner (Schmucker, 1970) to form the pair of real and quadrature induction arrows, for

graphical presentation. On these maps the directions of real arrows have been reversed so as to point towards the region of high conductivity that causes the concentration of induced currents. Consistent with the e^{iwt} time representation followed in the Fourier transformation, signs of the quadrature (out-phase) arrows have also been reversed (Lilley and Arora, 1982).

4. Principal Induction Features

4.1 Induction arrow pattern at short periods

The salient induction features which help to outline the conductive structures of the study region are seen on the arrow maps of short periods, e.g. at 12 min period in Fig. 2. The most conspicuous induction pattern are summarized below:

(I) On the eastern profile, SE-pointing real induction arrows at STE, COC, SIN and BAC, combined with the reversed arrows at BBR and SJP, are a diagnostic evidence of a conductive structure running approximately NE-SW between these two groups of stations. This conductive zone confined mostly to the southeastern part of the array is henceforth referred to as the Parnaíba Basin Conductivity Anomaly (PBCA). A rather unusual but persistent feature of the arrow pattern associated with the PBCA is that, near the central part of this anomaly, the induction arrows at ARC and BVI point away rather than pointing towards the central axis. This arrow pattern is considered to mark localized heterogeneity, such as the presence of a localized resistive body embedded within the PBCA. On the other hand, the quadrature arrows along the eastern profile (Fig. 2), with their parallel and anti-parallel behavior to the real arrow pattern, indicate the 2-D character of the involved structure (Chen and Fung, 1985). In fact, the presence of a localized resistive structure in the central part of the PBCA is more conspicuously indicated by the large and oppositely directed quadrature arrows at BAC and ARC and also help to locate the NW edge of the PBCA between COC and SIN, and the SE edge between BVI and BBR, respectively.

(II) The near north pointing arrow at BRA represents conventional geomagnetic coast effect related to the concentration of induced currents in the conducting sea water. Moving inland, the S-

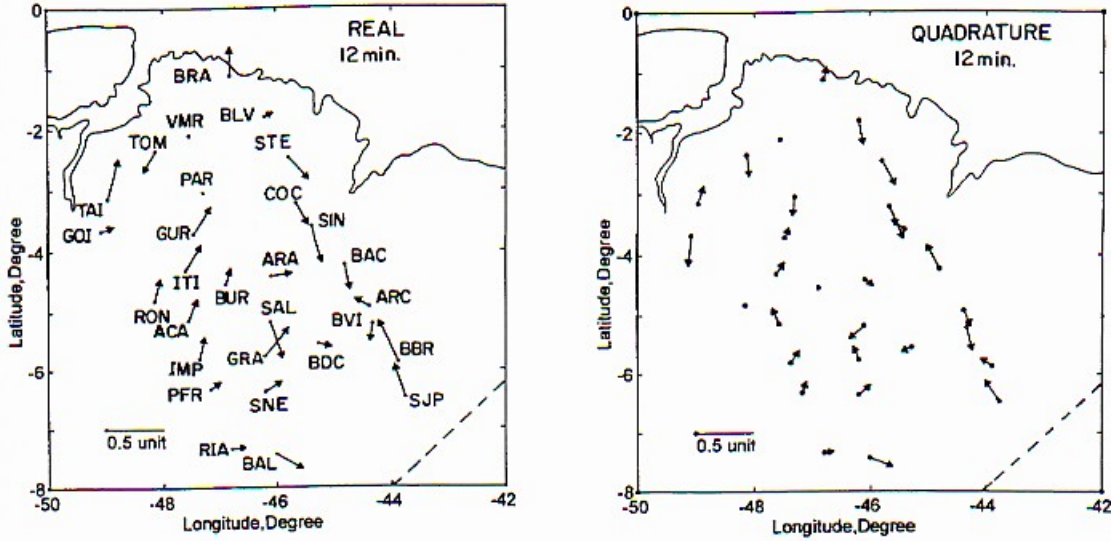

Fig. 2. Real and quadrature induction arrows corresponding to the period of 12 min.

SW pointing arrow at TOM, as opposed to the general N-NE directed arrows at TAI and on other stations on the western part of the array, suggests the presence of another elongated structure with its axis located between TOM and TAI. The structure appears to extend SE to produce a near zero magnitude arrow at PAR. This anomalous pattern extending from the region of the Marajó Basin towards the Parnaíba Basin is named LINK anomaly. The accompanying quadrature arrows, although weak compared to their counterparts, warrant nearly identical inference on the lateral conductivity distribution over the northwestern part of the array.

(III) The reversal of induction arrows between GRA and SAL is indicative of a localized linear structure saddling between this pair of stations. Both the real and quadrature arrows at BAL consistently have SE orientation but the absence of stations further SE, fails to locate the extent and location of the current concentration associated with this induction feature.

4.2 Period dependence of induction arrows

Examination of Fig. 3 shows that the induction picture seen at the period of 12 min undergoes systematic changes with increasing period. With increasing period (e.g., see map for 43 min period in Fig. 3), the induction arrows at BLV, STE and COC, on the NE part of the array, swing to a direction perpendicular to the nearest coast line. The geographical area over which this rotational behavior is noticed increases gradually, until at periods of 79 min (Fig. 3) or higher the arrows at all array stations tend to point uniformly in the NE direction. This behavior suggests that induction features at long periods are totally controlled by the currents in the deep ocean located some 500–600 km away from the center of the array. However, the quadrature arrows do not exhibit this rotational dependence on the period. Instead, even at these long periods, they continue to define the conductive structures, identified by the short period arrows. This varied period-dependence of the real and quadrature behavior may manifest from the electrical character. either reactive or resistive, of the conductors carrying induced currents (Gough *et al.*, 1974). The real arrows at these long periods point towards the ocean, as might be expected for induction in a highly conducting sea water wherein the reactive inductance exceeds the resistance, so the induced fields are in-phase with the inducing fields (Gough and Ingham, 1983). In contrast, the induction in sedimentary basins, where marked phase differences would occur between induced and inducing fields due to the dominance of resistance rather than inductance, the quadrature arrows would point towards such induced current. It is interesting that both in terms of period and spatial behavior, the situation is similar to the case in South Australia where Chamalaun (1985) observed real arrows for periods comparable to the long period of 79 min shown in Fig. 3. persistently pointing towards the nearest continental shelf margin but at short periods of 15–20 min swing away from the coast to indicate a conductive zone beneath the Houghton anticlinal zone. Another example showing that if large conductivity structure produces consistently large real induction arrows over sufficiently long distances then its position could be up to hundreds of kilometers distant from the observing stations, was discussed by Arora *et al.* (1982) in a context of induction pattern observed over the lower part of the NW India array.

4.3 Polarization dependence of induction anomalies

By 'playing back' the hypothetical event analysis (Bailey *et al.*, 1974) on the vertical field transfer functions, the real (ZR) and imaginary (ZI) parts of the anomalous vertical field that would be generated by horizontal fields of unit amplitude in a given azimuth were obtained. Figure 4 gives the contour maps of the ZR at the period of 12 min when the horizontal fields were polarized N30°W and N60°E. A distinct pattern with closed positive and negative vortex is seen over the southeastern part, associated with the PBCA. This anomalous pattern is best developed when horizontal field is polarized N30°W and almost diffuses on the map with orthogonal polarization, which shows another distinct pattern in the northwestern part. The latter double vortex pattern, related to the LINK anomaly, is found to be strongest for the polarization of N30°E (not

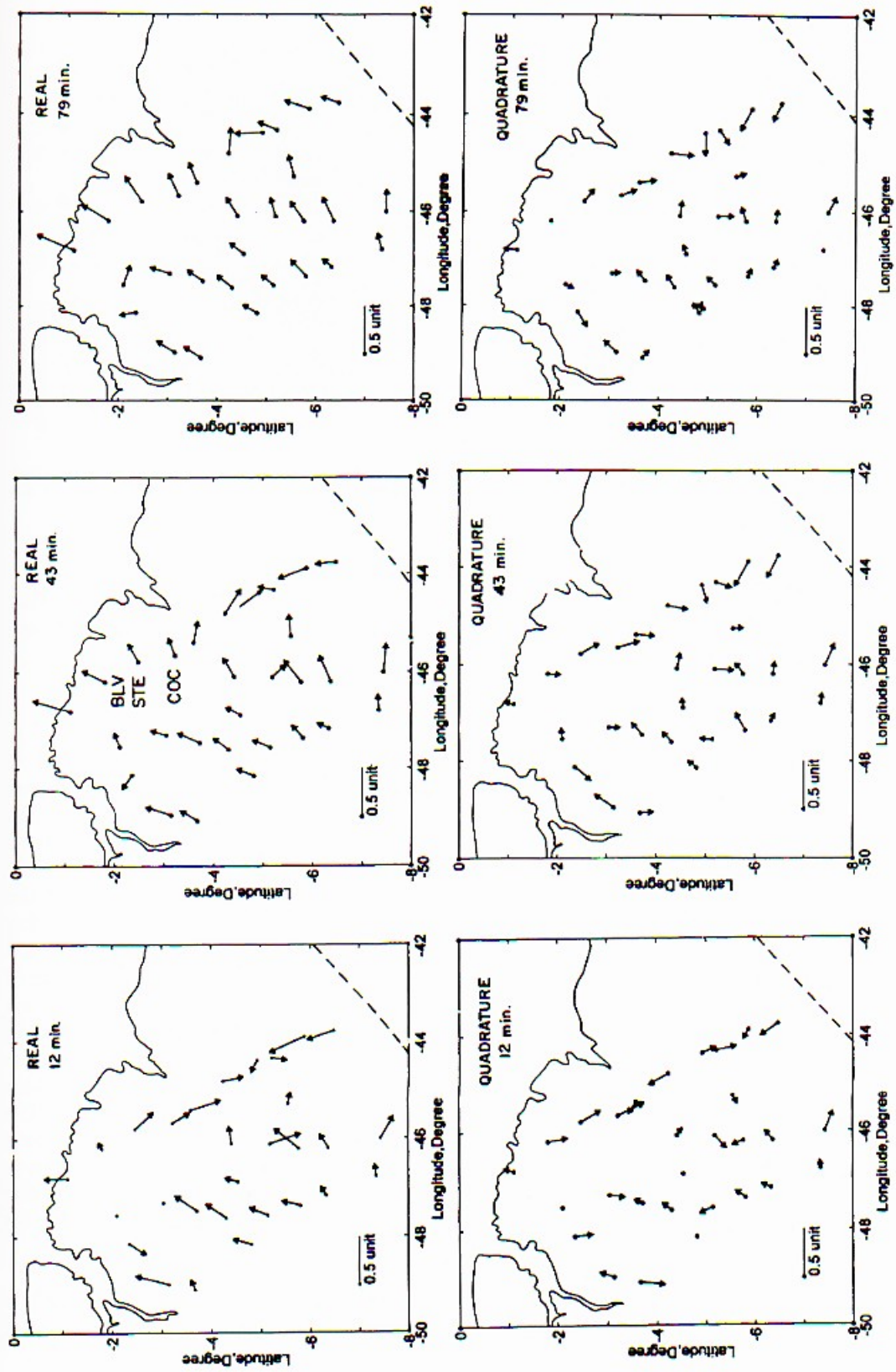

Fig. 3. Real and quadrature induction arrows for three periods: (a) 12 min, (b) 43 min, and (c) 79 min.

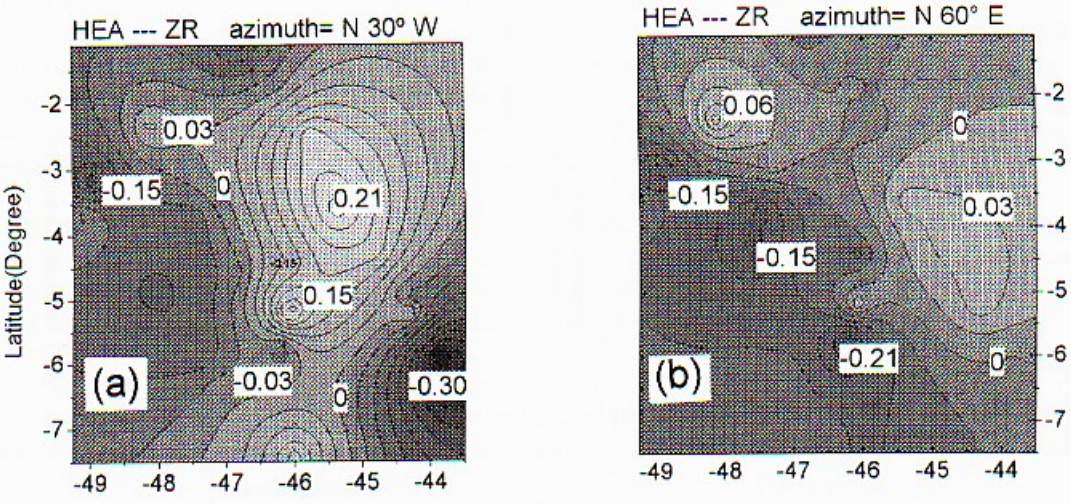

Fig. 4. Contour maps of the real part of the anomalous vertical field (ZR) produced by horizontal fields polarized along the (a) N30°W and (b) N60°E. Contour interval is 0.03 nT and only zero and extreme values of ZR are denoted.

shown) and corresponding minimum is noticed for the polarization of N60°W. These polarization sensitive responses are a clear indication that structurally the PBCA and the LINK anomaly are related to the elongated structures striking respectively N60°E and N60°W.

5. Thin Sheet Modelling

A 3-D thin sheet formulation developed by Vasseur and Weidelt (1977) has been used to model and interpret the observed electromagnetic response of a variety of conductive structures indicated by the induction arrow maps. Modelling at the longer periods to incorporate the induction effects of the distant currents flowing in the Atlantic ocean would require the inclusion of a very large geographical area. Given the large computer memory requirement, this could be achieved only by choosing relatively large node spacing, a parameter that would restrict the resolution of the shorter wavelength inland anomalies. As a trade-off between these contrasting requirements, the thin sheet model has been worked out at a period of 12 min, where the inland anomaly patterns are best developed. For this modelling, a 44 × 44 grid with a node spacing of 27.5 km, covering roughly an area of 11° × 11°, was considered. The included area is still much larger than the actual observational domain to allow incorporation of important neighboring tectonic elements. The continental shelf and included oceanic region also helps to reproduce the coast effect, which is small and does not extend to far distances landward at short periods. This thin sheet is considered to overlie a four layer earth model, shown in the lower part of Fig. 5. The choice of the deep layered structure was based on the geoelectrical model determined by a long period MT sounding made at the station MAU (Stoerzel, 1996), some 200 km east of the array station BAC (location shown in Fig. 1). In compliance with the requirement of the Vasseur and Weidelt's (1977) formulation, the normal structure surrounding the working anomalous domain was represented by a medium with conductance of 80 S.

5.0.1 Conductance assignment

In the theoretical formulation, the thin sheet has infinitesimal thickness, in the sense that it is characterized by laterally variable conductance only. However, it is usual to assign an equivalent

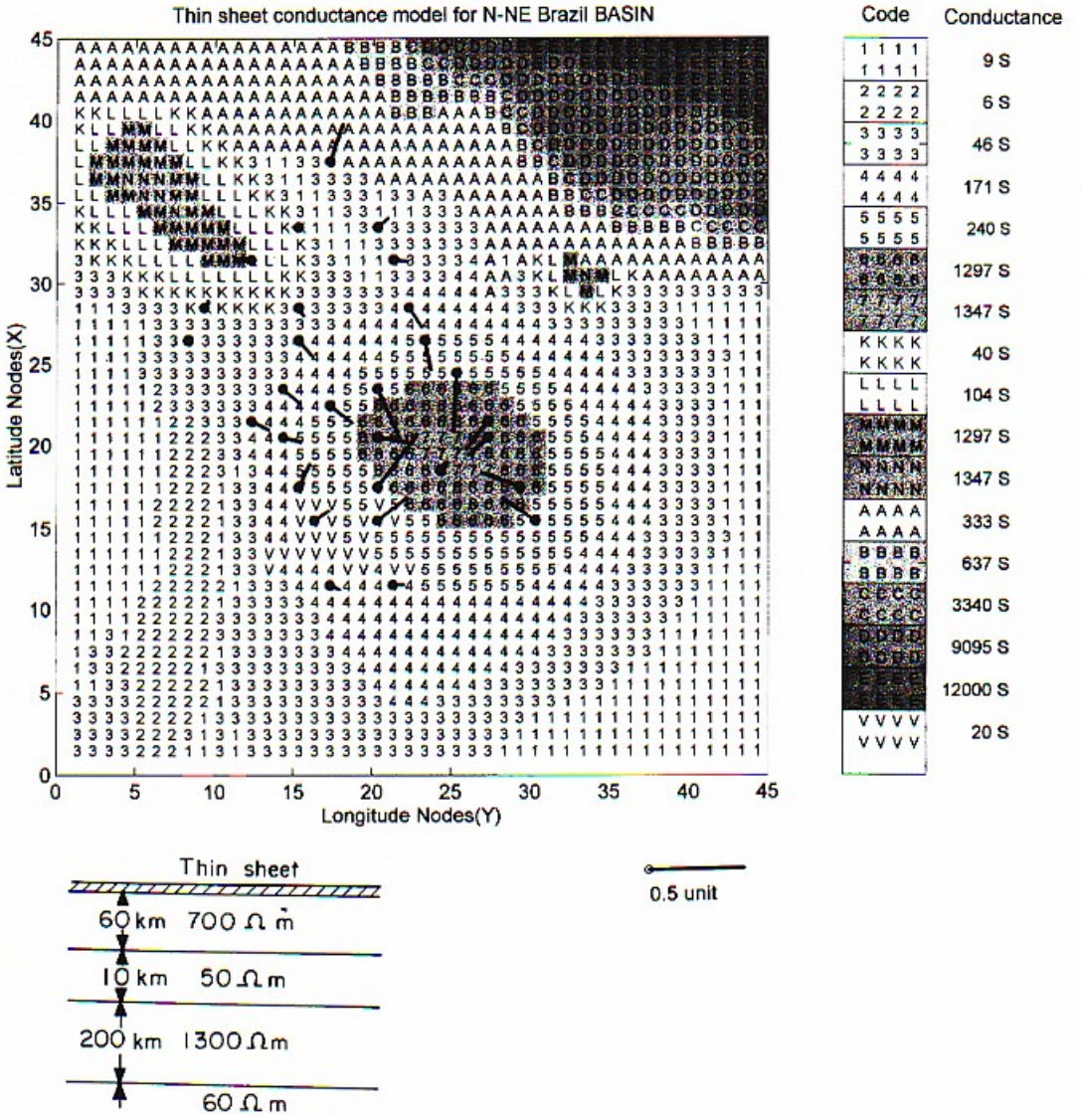

Fig. 5. Thin sheet conductance map for the Basin model. Conductance codes and their conductance values, as defined in Table 1, are also indicated. Gray shades distinguish zones of different conductances. Resulting response at the 12 min period is shown by the induction arrows only for the nodes representing the magnetometer sites. Also shown at the bottom is the layered structure beneath the thin sheet.

thickness, such that conductances may be thought of as conductivity integrated vertically through the thickness of the material which the sheet represents (Vasseur and Weidelt, 1977; Agarwal and Weaver, 1989; Arora *et al.*, 1993). The available information on the lithology and electrical character of the medium over the thickness of the sheet can be a useful guide to assign the initial conductance to the cells into which the working grid is divided. The process also proves helpful in the geological interpretation and in ascertaining the physical causes of high conductances. The thickness of 6 km was considered appropriate for the thin sheet as it allowed for a reasonable

incorporation of the thick strata of inland sediments, and also the ocean and conductive sediments beneath the ocean floor. Assignment of conductances to the cells outlining the Parnaíba basin was guided by magnetotelluric (MT) results and also took into account the available information on the lithological character. Extensive MT surveys in the adjoining contemporary Paraná basin by Stanley *et al.* (1985) have shown that the Paleozoic sequence is characterized by resistivity of 3–12 Ωm. The resistivity of 7 Ωm (central value of 3–12) was adopted to characterize the Paleozoic sequence, represented jointly by the Serra Grande and Canindé Groups of rocks. This uniform low resistivity value is consistent with the shale dominated lithology of both Serra Grande and Canindé groups of sediments (Mesner and Wooldridge, 1964; Góes *et al.*, 1990). Consistent with the semi-arid environment of deposition during the third cycle, sand dominated Balsas Group and the overlying Mesozoic sediments were assigned moderate resistivity of 30 Ωm. Further for the purpose of determining the conductances of cells, the estimate on the thickness of individual formations in various isopach zones was obtained from the borehole constraint geological cross-section (Góes and Feijó, 1994).

The conductances in the region of the Marajó basin were similarly computed, taking into cognizance that a large part of the basin is filled with Mesozoic and Cenozoic sediments although Paleozoic sediments are known to be preserved in the graben under the cover of Cretaceous and Tertiary sediments. The crystalline shield region was assigned a conductance equivalent to the resistivity (700 Ωm) of the substratum, symbolizing basement beneath the thin sheet. The Araguaia fold belt was assigned a very low conductance of 6 S to depict its resistive character.

The conductances of the cells over the ocean region were proportional to the mean depth of sea water between successive bathymetric contour lines. The conductivity of the sea water was taken to be 0.33 Ωm (Heinson and Lilley, 1993). However, in the shelf region where the sea depth is less than 1000 m, 250 m of conducting (1 Ωm) sediments were added to the water column for the purpose of defining the conductances for cells marked by codes A and B in Figs. 4 and 5. Inclusion of 250 m thick sediments beneath the sea floor helped to reproduce reasonably well the induction arrow at BRA.

Table 1 gives the contribution of different lithologies and/or sea water to the conductance of the various conductivity codes (cells) used to define the thin sheet model for north-northeast Brazil.

5.0.2 Physical validation of boundary conditions

The different categories of conductances as well as geometrical parameters (thickness and grid size) of the thin sheet satisfied the following conditions necessary to validate the thin sheet approximation (Weaver, 1982):

(i) The skin-depth (δ) in the layer immediately beneath the thin sheet is 350 km for the modelling period of 12 min. The assumed thickness of the thin sheet (h = 6 km) is much less than the stipulated limit of 15% of δ.

(ii) At 12 min period, the skin-depth (η) in the most conductive inland cell (2000 S) is 22.9 km and satisfies the condition $(h/\eta)^2 \ll 1$. The skin depth of 9.3 km in the sea water exceeds the maximum depth of water column by 2–3 times. Elsewhere on the sheet with lower conductance, $(h/\eta)^2$ would be much less than one, ensuring that the thin sheet conditions are satisfied everywhere, both on the land and in the oceanic region.

(iii) The grid spacing is 27.5 km and satisfies the condition that it should be less than $\delta/3$.

5.1 Basin model

In order to test the extent to which known information on the Parnaíba and Marajó basins coupled with induction in the ocean can account for the observed induction pattern, the initial thin sheet model developed considered the spatial distribution of conductances based only on the isopach and bathymetry shown in Fig. 1. Figure 5 shows in coded form the surface distribution of conductances so developed. The real induction arrows resulting from induction in the thin sheet

Table 1. Conductances associated with various codes used to define the thin sheet model for N-NE Brazil (Fig. 6) and their contributing sources.

Conductance Code	Contributing Lithologies			Cell Conductance
	Mesozoic h_1/ρ_1	Paleozoic h_2/ρ_2	Basement h_3/ρ_3	$\sum h_i/\rho_i$
Parnaíba basin				
3	300/30	200/7	5500/700	46 S
4	450/30	1050/7	4500/700	171 S
5	800/30	1700/7	3500/700	275 S
8, 9		Variable		2000 S
For BASIN model	(Fig. 5)			
5*	800/30	1450/7	3750/700	240 S
6*	900/30	(1850/7+1000/1)	2250/700	1297 S
7*	900/30	(2200/7+1000/1)	1900/700	1347 S
Marajó basin				
K	1000/30	—	5000/700	40 S
L	3000/30	—	3000/700	104 S
M	5000/30	—	1000/700	168 S
N		Variable		1000 S
Ocean	Sea water	Sediments	Basement	
A	25/0.33	250/1	5725/700	333 S
B	125/0.33	250/1	5625/700	637 S
C	1100/0.33	—	4900/700	3340 S
D	3000/0.33	—	3000/700	9095 S
E	4000/0.33	—	2000/700	12000 S
Other regions				
1	Precambrian rocks			8.6 S
2	Araguaia fold belt			6.0 S
S	Conductive zone			2400 S
R	Conductive zone			1200 S
Y	Extension zone			460 S
V	Volcanics			20 S
I	Intrusive diabase			20 S

at the 12 min period are also superposed, only for the nodes representing observational sites on the numerical grid. The comparison with the observed pattern in Fig. 2 showed that the calculated response provides a poor fit to the observation. Only on the eastern profile some resemblance to the observation is seen, but also only in the direction of the arrows. The most significant differences are seen on the western half of the array. Here, in contrast to the observed N-NE directed arrows, the calculated arrows with their SE orientations point towards the central part of the Parnaíba basin. This mismatch warrants a very complex conductivity distribution beneath the western part, whereas elsewhere disagreements may manifest the unknown local variation in thickness and conductivity of sediments, or contribution from deeper portions of the crust.

5.2 Regional model

The basin model previously discussed, which considered the spatial distribution symmetric with respect to the deepest part of the Parnaíba basin and closely following the isopach contours, could not explain the most salient features of the observed arrow pattern. To obtain agreement

between the observed and calculated response, conductances of certain cells, particularly in the central part of the Parnaíba and Marajó basins, and their lateral configurations were changed in a number of experiments. Figure 6 shows in coded form the distribution of depth-integrated conductances, whose induction responses reproduce the observed induction pattern quite satisfactorily. The overall induction picture resulting from induction in the thin sheet of Fig. 6 at 12 min period is shown in Fig. 7 for all nodes of the working grid. The comparison of the model and the observed arrows, both for real and quadrature parts, is shown in Fig. 8. The modelled real and quadrature arrows reproduce fairly well the gross features of the observed pattern.

5.2.1 Parnaíba Basin Conductivity Anomaly (PBCA)

In the attempt to reproduce both directional and spatial magnitude pattern along the eastern profile, the thin sheet model approximates the PBCA roughly as a NE-SW elongated structure. In particular, the NE continuation of the section of the PBCA (marked by code 9 in Fig. 6) helps to reproduce the SSE pointing arrow at BAC, which otherwise points SW, towards the center. This extension also gives the PBCA a two-dimensional character, which is consistent with the polarization dependence of the observed induction response discussed earlier. The introduction of a low conductance (resistive) strip within the PBCA reproduces the reversal of arrows at ARC

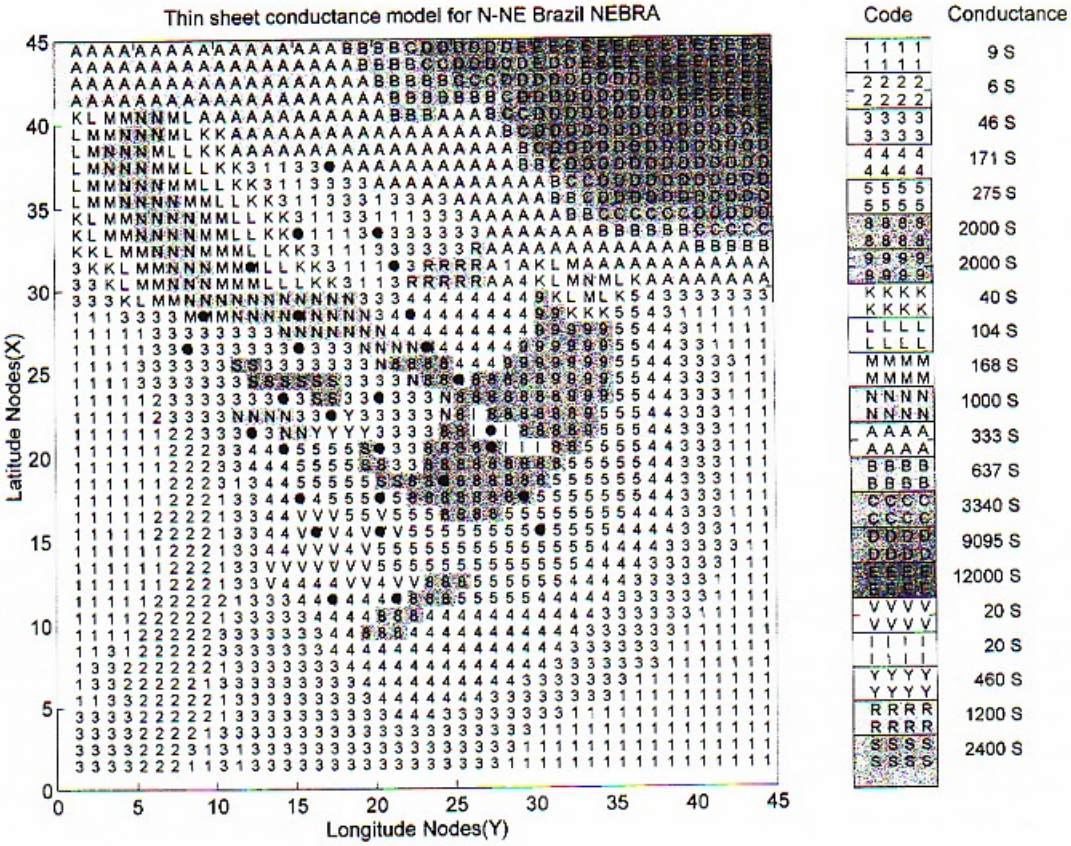

Fig. 6. Thin sheet conductance map for the Regional model of north-northeast Brazil. Conductance codes and their conductance values, as defined in Table 1, are also indicated. Gray shades distinguish zones of different conductances. Darker shades denotes mapped high conductivity zones. Nodes representing magnetometer sites are marked by solid circles.

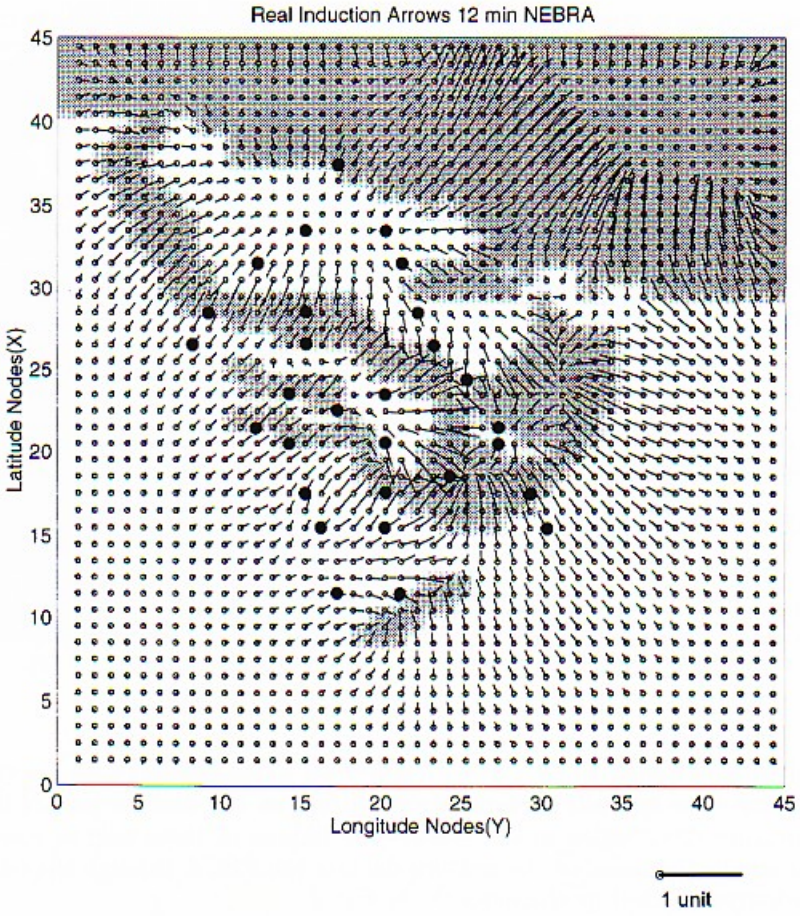

Fig. 7. Real induction arrows resulting from induction in the thin sheet model shown in Fig. 6 at the 12 min period. Induction arrows are shown for all nodes of the working grid. Magnetometer sites are also marked by solid circles.

and BVI. A linear NW extension of the PBCA, on the western flank, is able to account for the sharp reversal of the induction arrows between GRA and SAL.

5.2.2 LINK anomaly

In the NW part, when the conductivity distribution in the Marajó basin was solely guided by the isopach the resulting induction pattern fails to reproduce the reversal of the arrows between TOM and TAI (Fig. 5). However, when the conductivity distribution is allowed to follow the graben structure bounded by normal faults (shown in Fig. 1), the resulting arrow pattern reproduces the reversal between TOM and TAI (Figs. 6 and 7). The extension of this conductive zone in the SE direction is able to account for the near-zero magnitude real induction arrow at PAR and the N-NE pointing arrow at GUR. The connectivity of this high conducting zone to the main PBCA is needed in order to produce the E-NE pointing arrow at ARA and a minor but significant deviation of the arrow at COC from the regional arrow directional pattern on the eastern profile.

On the central-western part of the array, a model response consistent with the observation was achieved by incorporating two narrow conductive strips, sub-parallel to the LINK anomaly.

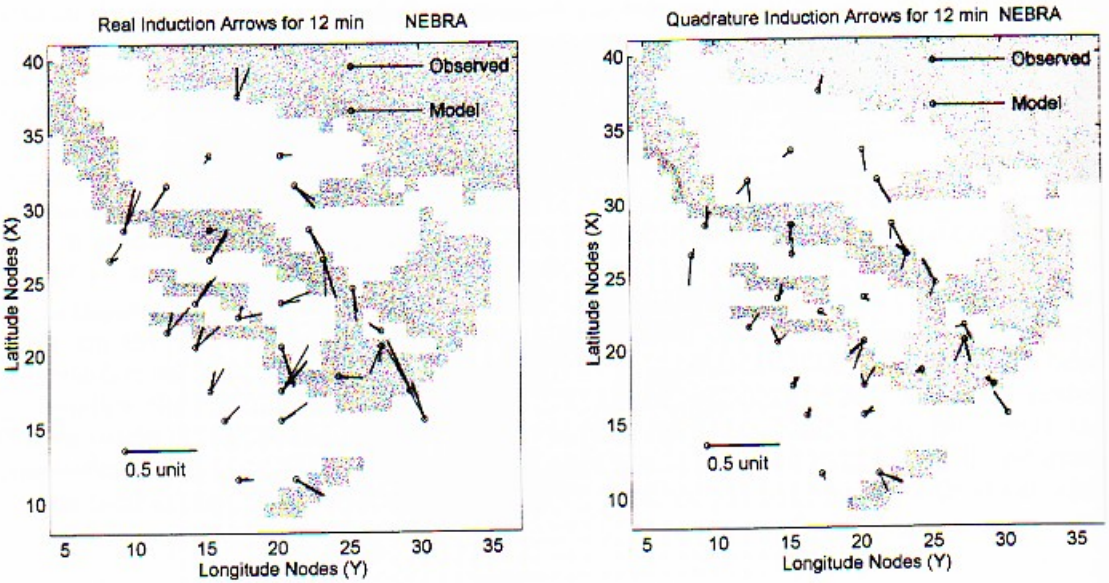

Fig. 8. Comparison of observed and model induction arrows for the 12 min period. Shaded area denotes high conductance zones mapped by the thin sheet model.

Perhaps the aliasing of induction effects of these narrow strips coupled with the response of the LINK anomaly gives the spatially uniform arrow pattern on the western part of the array. The inferred conductance distribution model favours the linkage of these narrow conducting strips with the linear conducting zone on the western flank of the PBCA through the only moderately conducting pathways, marked by character 'Y' in Fig. 6.

5.2.3 Minor conductive features

To a great extent, the most salient induction arrow patterns at short periods could be explained by currents circulating in the sediments of the Parnaíba and Marajó basins, and in the ocean. There are, however, some minor unexplained features, e.g. the SW pointing arrow at BAL. A NE-SW conductive structure, with a conductance equivalent to that of the PBCA, is able to reproduce the arrow at BAL similar to the observation.

A little enhanced conducting zone (marked by code R in Fig. 6) was required to account for the SW pointing arrow at STE. This structure may be viewed as the sub-surface elongation of the São Luiz basin carrying older Paleozoic or Cretaceous sediments under the cover of the more recent Cenozoic sediments.

6. Tectonic Implications and Possible Sources of Enhanced Conductivity

The overall picture of the deduced depth-integrated conductivity for the study region is shown in Fig. 9. In contrast to the surface oval shaped physiography of the Parnaíba basin, the inferred conductivity distribution suggests a complex structural configuration at depth. Although the depth of the involved structures is not resolved by the thin sheet modelling, the MT soundings carried out along a 70 km profile (shown as MT1 in Fig. 1) have identified a layer of high conductivity (<1 Ωm) within the basin at a depth of about 1800 m (Oliveira and Fontes, 1991). This high conductance layer acted as a shield for diffusing electromagnetic waves for the entire frequency band (500 Hz to 0.001 Hz) of measurements, inhibiting information on the deeper

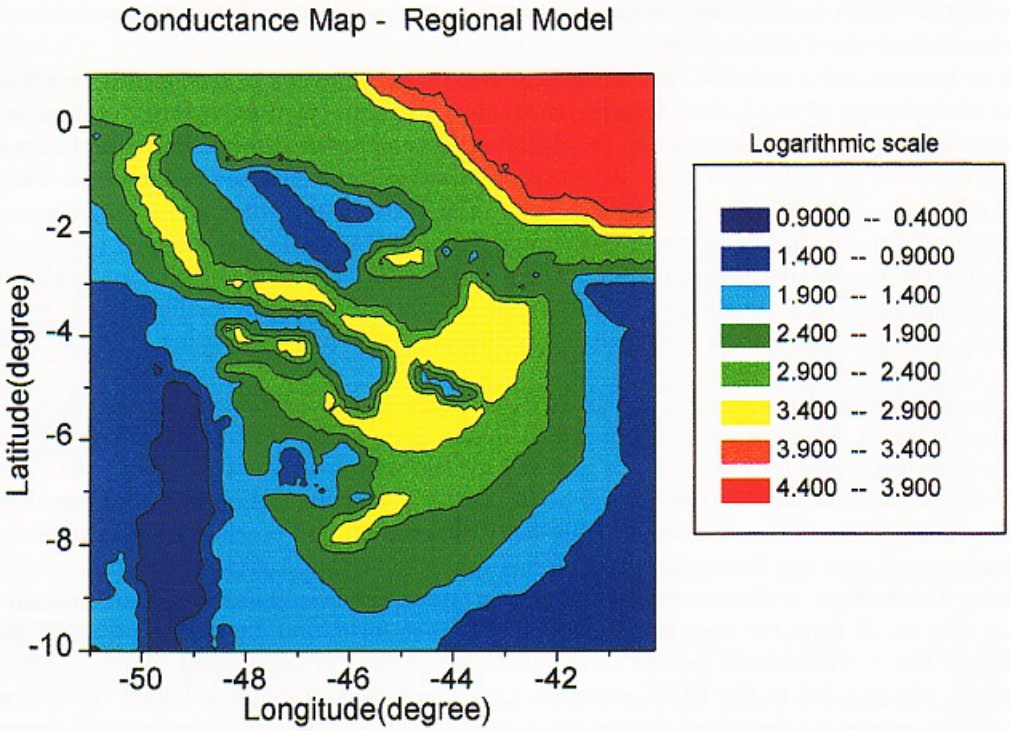

Fig. 9. The spatial variation of conductances (logarithmic scale) in the study area as deduced from the thin sheet modelling.

sediment-basement configuration. However, the MT soundings on another profile near the SE fringe of the basin (MT2 in Fig. 1) indicate the presence of a relatively less conducting layer of 10 Ωm above the sediment-basement interface (Lima *et al.*, 1996). This suggests that the highly conductive zone is located within the basin, primarily confined to its central part. Given the sensitivity of the GDS technique to locate the lateral electrical contrast, the thin sheet model has outlined the spatial extent of this anomalously high conductivity layer in the central part of the basin (PBCA). The mapped distribution suggests that the most dominant pattern is marked by a NE-SW trend on the north-eastern part of the basin, perhaps signifying the control of a major Precambrian basement structure on the evolution of the Parnaíba basin. The possible existence of the NE-SW trending structure in the basement had earlier been envisaged by Nunes (1993), based on gravity, aeromagnetics and other related data. It also corroborates the hypothesis of Góes *et al.* (1990) that prior to the subsidence of the Parnaíba basin, which began in late Ordovician or early Silurian, the tectonic forces associated with the final pulse of the Braziliano orogenic cycle had led to the development of a graben structure, trending NE-SW, in the region where the basin was to form. The graben formed the seat for the deposition of the Cambro-Ordovician series, containing carbonates with high carbon, shale with oölitic limestones and subgraywacke sandstones (Mesner and Wooldridge, 1964). It seems that these slightly metamorphosed carbon-rich carbonates could be the possible source of the enhanced conductivity. The parallelism of the PBCA and the observation that its SE edge is limited by the Transbrasiliano lineament, is another evidence of the control of the NE-SW oriented tectonic elements on the evolution of the Parnaíba basin from the early stages. The linear elongated conductive belt, giving an arcuate

shape to the PBCA on the lower western flank (Fig. 9), perhaps mark the narrow inlets of sea intrusions where the Cambro-Ordovician strata are best preserved.

The presence of a resistive belt within the PBCA is indicative of localized heterogeneities in the central part of the basin. Ussami *et al.* (1993) examining the isostatic residual gravity anomaly map in the regional tectonic perspective, viewed the area of the Parnaíba basin as an annular low with an embedded high. Given the tectonic scenario that the region of the Parnaíba basin, following sedimentation from Ordovician to the Tertiary, has witnessed a major magmatic event during Jurassic to Cretaceous (Mesner and Wooldridge, 1964), the mapped resistive body enclosed in the conductive environment may be a diabase intrusive related to the magmatic event. The entrapment of this resistive structure in the conductive host has facilitated its detection, although induction studies are more suited to delineate the conductive rather than the resistive bodies (Jödicke, 1992).

The location and orientation of the LINK anomaly is appropriate to suggest that it may represent relics of sedimentary channels which might have connected the Marajó and Parnaíba basins. This link could have served as a gateway for the transgression of the sea to the Parnaíba basin via the Amazon through the Marajó basin. Perhaps, this connection was established during the Devonian, when the areal extent of the sea transgression had reached its maximum extent and had crossed over the Tocantins arch (Mesner and Wooldridge, 1964). The nature of the conductivity distribution on the western part of the array suggests a complex basement configuration such as may result from the deep seated folding or graben formation during the period of general subsidence and sedimentation related to the evolution of the Parnaíba basin. Areas of high conductances, sub-parallel to the LINK anomaly, may mark fault grabens or folded troughs where sedimentary sequences deposited during the period of the sea transgression are still preserved, whereas intervening zones mark regions of uplift and erosions during intervals of sea regression.

A narrow NE-SW trending conductance zone, introduced in the thin sheet model to explain the behavior of the induction arrow at BAL, is aligned with the Transbrasiliano lineament where the existence of grabens infilled with sediments older than the Serra Grande Group, i.e. Cambro-Ordovician, has been inferred based on MT and gravity data (Sousa and Oliveira, 1995). The carbon-rich carbonates of the Cambro-Ordovician strata constitute the potential candidates for the mapped high conductivity zones. Based on the borehole lithology, Bigarella (1973) has also reported the occurrence of black shales in the Pedra De Fogo formations of Permian age. These black shales would also be a significant contributor to the high conductance.

7. Conclusions

The array experiment has been useful by providing a gross picture of the electrical conductivity distribution in the Parnaíba basin and contiguous region. Contrary to the believed peneplane character of the basement, the inferred conductivity distribution suggests that the basement has been corrugated by troughs and grabens where sedimentary remnants are still preserved. The presence of highly conductive sediments in the central deeper parts of the basin (PBCA) is consistent with the MT surveys, but the array data have permitted the mapping of the lateral extent of the PBCA in greater detail. The mapped configuration favours the development of a NE-SW graben structure linked to the onset of a regional subsidence in the area where the basin was to be formed later. The mapped conductivity distribution also provides strong geophysical evidence on the connectivity of the Parnaíba basin to the Marajó basin, which might have served as a gateway for the intrusion of the sea during some part of the evolution of the Parnaíba basin. However, the vertical structure of this LINK anomaly and other inferred anomalous zones, largely remain unresolved. New MT inputs would significantly improve the vertical resolution. But as emphasized by Egbert and Booker (1993), the success with MT requires detailed mapping with closely spaced electrical field measurements, which in practice restricts collection of data on a limited number

of two-dimensional profiles. On these counts, information provided by the present exercise could be helpful in locating the transects as well as the frequency band of MT measurements. Broad-band MT measurements along two profile running across the PCBA and LINK anomalies, which can penetrate through the indicated highly conducting strata and can even provide information on deeper crustal structures, would be helpful in further elucidating the tectonic and structural evolution of the intracratonic Parnaíba basin.

This work forms part of the Conselho Nacional de Desenvolvimento Científico e Tecnológico (CNPq) funded Project No. 522342/94-9 entitled '*Equatorial Electrojet Related Electromagnetic Induction*'. One of the authors (B.R.A.) is also thankful to the CNPq for the award of a Visiting Research Fellowship. Another author (A.R.) was the recipient of a CNPq Overseas Doctoral Fellowship to work at the Flinders University of South Australia. The support provided by G.D. Prasad, INPE, with the MATLAB graphics is gratefully acknowledged. The authors also thank Markus Eisel and an anonymous referee for their helpful suggestions.

REFERENCES

Agarwal, A. K. and J. T. Weaver, Regional electromagnetic induction around the Indian Peninsula and Sri Lanka: a three-dimensional numerical model using the thin sheet approximation, *Phys. Earth Planet. Inter.*, **54**, 320–331, 1989.

Almeida, F. F. M. de, Sistema tectônico marginal do Cráton do Guaporé, *Proc. XXVIIIth Congresso Brasileiro de Geologia*, Porto Alegre, Brazil, V. 4, 9–17, 1974.

Almeida, F. F. M. de, Y. Hasui, B. B. de Brito Neves, and R. A. Fuck, Brazilian structural provinces: an introduction, *Earth Sci. Rev.*, **17**, 1–29, 1981.

Arora, B. R., F. E. M. Lilley, M. N. Sloane, B. P. Singh, B. J. Srivastava, and S. N. Prasad, Geomagnetic induction and conductive structures in northwest India, *Geophys. J. R. Astron. Soc.*, **69**, 459–475, 1982.

Arora, B. R., P. Kaikkonen, M. V. Mahashabde, and S. Y. Wahgmare, A non-uniform thin sheet model for geomagnetic induction anomalies in central India, *Phys. Earth Planet. Inter.*, **81**, 201–213, 1993.

Bailey, R. C., R. N. Edwards, G. D. Garland, and J. P. Greenhouse, Electrical conductivity studies over a tectonically active area in eastern Canada, *J. Geomag. Geoelectr.*, **26**, 125–146, 1974.

Beamish, D., The mapping of induced currents around the Kenya rift: A comparison of techniques, *Geophys. J. R. Astron. Soc.*, **50**, 311–332, 1977.

Beamish, D. and R. J. Banks, Geomagnetic variation anomalies in northern England: processing and presentation of data from a non-simultaneous array, *Geophys. J. R. Astron. Soc.*, **75**, 513–539, 1983.

Bigarella, J. J., Geology of the Amazon and Parnaíba basins, in *The Ocean Basins and Margins, Vol. 1 - The South Atlantic*, edited by A. E. M. Nairn and F. G. Stehli, pp. 25–86, Plenum Press, New York, 1973.

Chamalaun, F. H., Geomagnetic deep sounding experiment in the Central Flinders Ranges of South Australia, *Phys. Earth Planet. Inter.*, **37**, 174–182, 1985.

Chamalaun, F. H. and J. D. McKnight, A New Zealand wide magnetometer array study, *J. Geomag. Geoelectr.*, **45**, 741–759, 1993.

Chamalaun, F. H. and R. Walker, A microprocessor based digital fluxgate magnetometer for geomagnetic sounding studies, *J. Geomag. Geoelectr.*, **34**, 491–507, 1982.

Chen, P. F. and P. C. W. Fung, Significance of the sign changing of the imaginary arrows in geomagnetic induction investigations, *Geophys. J. R. Astron. Soc.*, **80**, 257–263, 1985.

Cunha, F. M. B., Evolução paleozóica da Bacia do Parnaíba e seu arcabouço tectônico, M.Sc. thesis, Univ. Federal Rio de Janeiro, Rio de Janeiro, Brazil, 1986.

DNPM (Departamento Nacional da Produção Mineral), Mapa tectônico do Brasil - Escala 1:5,000,000, 1971.

Egbert, G. D. and J. R. Booker, Robust estimation of geomagnetic transfer functions, *Geophys. J. R. Astron. Soc.*, **87**, 173–194, 1986.

Egbert, G. D. and J. R. Booker, Imaging crustal structure in Southwestern Washington with small magnetometer arrays, *J. Geophys. Res.*, **98**, 15967–15985, 1993.

Góes, A. M. O. and F. J. Feijó, Bacia do Parnaíba, *B. Geoci. PETROBRÁS*, **8**, 57–67, 1994.

Góes, A. M. O., J. M. P. Souza, and L. B. Teixeira, Estágio exploratório e perspectivas petrolíferas da Bacia do Parnaíba, *B. Geoci. PETROBRÁS*, **4**, 55–64, 1990.

Gough, D. I. and M. R. Ingham, Interpretation methods for magnetometer arrays, *Rev. Geophys. Space Phys.*, **21**, 805–827, 1983.

Gough, D. I., M. W. McElhinny, and F. E. M. Lilley, A magnetometer array study in southern Australia, *Geophys. J. R. Astro. Soc.*, **36**, 345–362, 1974.

Heinson, G. S. and F. E. M. Lilley, An application of thin sheet electromagnetic modelling to the Tasman Sea. *Phys. Earth Planet. Inter.*, **81**, 231–251, 1993.

Jödicke, H., Water and graphite in the earth's crust—An approach to interpretation of conductivity models, *Surv. Geophys.*, **13**, 381–407, 1992.

Lilley, F. E. M. and B. R. Arora, The sign convention for quadrature Parkinson arrows in geomagnetic induction studies, *Rev. Geophys. Space Phys.*, **20**, 513–518, 1982.

Lima, J. P. R., M. F. B. Oliveira, S. L. Fontes, and M. A. Meju, Evidência do lineamanto Transbrasiliano na Bacia do Parnaíba utilizando o método magnetotelúrico, *Proc. XXXIXth Congresso Brasileiro de Geologia*, Salvador, Brazil, V. 2, 372–375, 1996.

Mesner, J. C. and L. C. Wooldridge, Maranhão Paleozoic basin and Cretaceous coastal basins, North Brazil, *Bull. Am. Assoc. Petr. Geol.*, **48**, 1475–1512, 1964.

Nunes, K. C., Interpretação integrada da Bacia do Parnaíba com ênfase nos dados aeromagnéticos, *Proc. 3rd International Congress of the Brazilian Geophysical Society*, Rio de Janeiro, Brazil, V. 1, 152–157, 1993.

Oliveira, M. F. B. and S. L. Fontes, Magnetotelúrica na Bacia do Parnaíba: Primeiros resultados, *Proc. 2nd International Congress of the Brazilian Geophysical Society*, Salvador, Brazil, V. 1, 294–299, 1991.

Rezende, W. M. and J. O. Ferradaes, Integração geológica regional da bacia sedimentar da foz do Amazonas, *Proc. XXVth Congresso Brasileiro de Geologia*, São Paulo, Brazil, 203–214, 1971.

Rigoti, A., Geomagnetic array study of the EEJ in NE Brazil, Ph.D. Thesis, Flinders University of South Australia, 180 pp., 1994.

Schmucker, U., Anomalies of geomagnetic variations in the southwestern United States, *Bull. Scripps. Inst. Oceanogr.*, **13**, 1–165, 1970.

Sousa, M. A. and M. F. B. Oliveira, Geophysical evidences of the Transbrasiliano lineament in the Parnaíba basin, *Proc. Vth Simpósio Nacional de Estudos Tectônicos*, Gramado, Brazil, 260–263, 1995.

Stanley, W. D., A. R. Saad, and W. Ohofugi, Regional magnetotelluric surveys in hydrocarbon exploration, Paraná basin, Brazil, *Bull. Am. Assoc. Petro. Geol.*, **69**, 346–360, 1985.

Stoerzel, A., Estimation of transfer functions from magnetic variations of the equatorial electrojet—A method to determine static shifts in magnetotelluric data from equatorial latitudes, *J. Geophys. Res.*, **101**, 17,917–17,926, 1996.

Thompson, D. J., Spectrum estimation and harmonic analysis, *Proc. IEEE*, **70**, 1055–1095, 1982.

Ussami, N., N. C. De Sá, and E. C. Molina, Gravity map of Brazil: 2. Regional and residual isostatic anomalies and their correlation with major tectonic provinces, *J. Geophys. Res.*, **98**, 2199–2208, 1993.

Vasseur, G. and P. Weidelt, Bimodel electromagnetic induction in non-uniform thin sheets with an application to the northern Pyrenean induction anomaly, *Geophys. J. R. Astron. Soc.*, **51**, 669–690, 1977.

Weaver, P., Regional induction in Scotland: an example of three-dimensional numerical modelling using the thin sheet approximation, *Phys. Earth Planet. Inter.*, **7**, 266–281, 1982.